Université de Mons
Faculté Polytechnique – Service de Mécanique Rationnelle, Dynamique et Vibrations
31, Bld Dolez - B-7000 MONS (Belgique)
065/37 42 15 – georges.kouroussis@umons.ac.be

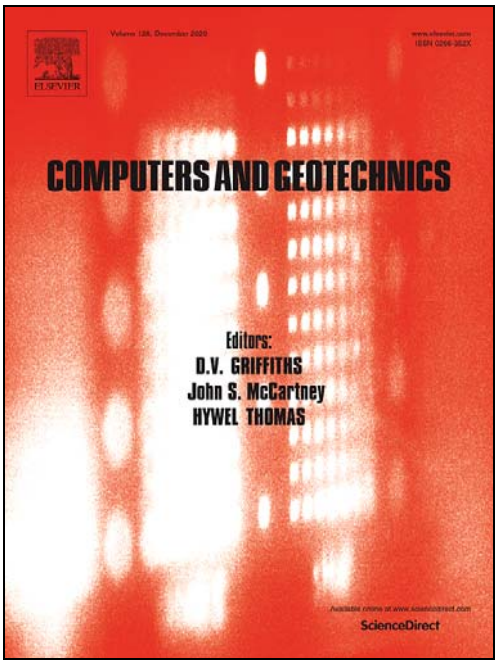

L. Qu, X. Ding, G. Kouroussis, C. Zheng, Dynamic interaction of soil and end-bearing piles in sloping ground: Numerical simulation and analytical solution, *Computers and Geotechnics*, 134C, 103917, 2021.

Computers and Geotechnics 134 (2021) 103917

Contents lists available at ScienceDirect

Computers and Geotechnics

journal homepage: www.elsevier.com/locate/compgeo

Research Paper

Dynamic interaction of soil and end-bearing piles in sloping ground: Numerical simulation and analytical solution

Liming Qu [a], Xuanming Ding [b,*], Georges Kouroussis [c], Changjie Zheng [d,e]

[a] MOE Key Laboratory of High-speed Railway Engineering, College of Civil Engineering, Southwest Jiaotong University, Chengdu 610031, China
[b] College of Civil Engineering, Key Laboratory of New Technology for Construction of Cities in Mountain Area, Chongqing University, Chongqing 400045, China
[c] Faculty of Engineering, Department of Theoretical Mechanics, Dynamics and Vibrations, Université de Mons, Belgium
[d] School of Civil Engineering, Fujian University of Technology, Fuzhou 350118, China
[e] Fujian Provincial Key Laboratory of Advanced Technology and Informatization in Civil Engineering, Fuzhou 350118, China

ARTICLE INFO

Keywords:
Sloping ground effects
Dynamic interaction
Wave propagation
Numerical simulation
Analytical solution

ABSTRACT

The effects of sloping ground on the vertical pile-to-pile interaction for end-bearing piles embedded in a homogenous soil are investigated through three-dimensional finite element simulations. The wave propagation mechanism and pile to pile interaction factor are investigated in detail from displacement and axial force perspectives. For contrast, soil attenuation and wave diffraction induced by a vertically vibrating end-bearing pile in horizontal ground are also studied. The highlight is put on the amplitude and phase lag in soil-pile system to reveal the essential characteristics of dynamic pile-pile interaction. Numerical results show that the dynamic displacement of a free field is position dependent. Moreover, the interaction factor of receiver pile on the upslope side is larger than the one on the downslope, since the longer embedded segment absorbs a greater amount of energy from the surrounding soil. On the basis of the numerical findings, an analytical model is established to calculate the dynamic responses of pile groups in sloping ground.

1. Introduction

Piles are generally subjected to dynamic loads from a range of sources such as vibrating machines, earthquake action, wind, or traffic vehicles, etc. The vibrating ('source') pile shaft can generate shear waves that will spread out and strike an adjacent pile (namely the 'receiver' pile), thereby imposing an additional vertical displacement on the receiver pile. The resultant displacement of receiver pile is significantly influenced by the amplitude and phase lag of striking waves which are dependent on the propagation distance and wavelength of the striking waves in soil medium. Specifically, when the waves arrive in an opposite phase with that of the source pile, the displacement of receiver pile is positively suppressed; when the waves arrive in approximately the same phase, that displacement is undesirably amplified. As a result, the dynamic stiffness at the pile head may be significantly reduced at certain frequencies and spatial locations, or be greater than the stiffness summation of all the individual piles (Wolf and Von 1978, Gazetas and Makris 1991, Wolf 1998). This is in contrast to the static pile-pile interaction, which always amplifies the displacement of the receiver pile (Poulos 1968, Randolph and Wroth 1978, Kanellopoulos and Gazetas 2019).

Due to the complex wave superposition process and potential aforementioned mechanism, the issue on calculating dynamic responses has received considerable attention in the past few decades. For the single pile case, soil attenuation factor φ is introduced to evaluate the attenuation effects of the free field vibration induced by the vibrating pile as shown in Fig. 1**(a)**. For the pile group, one of the most efficient methods to calculate the dynamic response is based on the concept of 'interaction factor' α_v that is defined as the ratio of the vertical displacement u_1 at the head of the loaded pile by the vertical displacement u_3 at the head of the receiver pile as shown in Fig. 1**(b)**.

Dobry and Gazeta (1988) proposed a practical and useful framework to calculate the "dynamic impedance of pile group", which is a critical physical quantity for engineering design and equals the ratio of the external force P_G acting on the cap to the induced cap displacement u_G during vibration as shown in Fig. 1**(c)**. In the study by Dobry and Gazeta (1988), the displacement u_3 of receiver pile was approached by the vertical displacement u_2 of the free field in position, i.e., $\alpha_v = \varphi$. That approximation gave a satisfactory estimation of interaction factor from a practical perspective, especially for the floating piles (Makris, and

* Corresponding author.
E-mail addresses: hustqlm@163.com (L. Qu), dxmhhu@163.com (X. Ding), georges.kouroussis@umons.ac.be (G. Kouroussis).

https://doi.org/10.1016/j.compgeo.2020.103917
Received 18 May 2020; Received in revised form 2 November 2020; Accepted 3 November 2020
Available online 31 March 2021

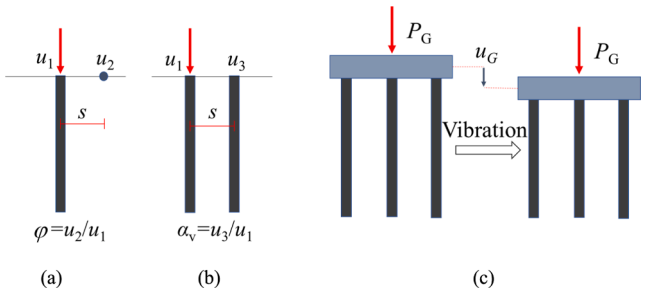

Fig. 1. Definition for soil attenuation factor, interaction factor and dynamic impedance of pile group (schematic). The symbol s is the distance of receiver position from loaded pile. (a) soil attenuation factor φ; (b) interaction factor α_v; (c) dynamic impedance of pile group (calculated by P_G/u_G).

Gazetas 1993). Furthermore, Mylonakis et al. (1998) introduced the concept of 'diffraction factor ζ' to consider the diffraction of the arriving wave field due to the rigidity of the passive pile and the interaction between pile and surrounding soil. As a consequence, α_v equals the product of soil attenuation factor and diffraction factor, i.e., $\alpha_v = \varphi\zeta$. Mylonakis et al (1988) elaborated the influences of axial stiffness of piles on the interaction factor, whereas the soil attenuation factor still requires the traditional plane strain assumption that neglects the vertical propagation of waves in soil. Taking account of the radial soil displacement and the vibration attenuation along vertical direction, Luan et al. (2019) deduced a rigorous three-dimensional solution for end-bearing group of piles in horizontal soil. More successful implementations involving dynamic pile-pile interaction in this domain were reported in Kanellopoulos and Gazetas (2019), Gazetas et al. (1993), Ullash et al. (2018), Zhang et al. (2019), etc.

In the recent years, increasing engineering projects of pile foundations for bridges, embankments and transmission towers locate in sloping topography (Lin and Yang 2013, Zhao et al., 2014, Nontapat et al., 2018, Lei et al., 2019). It is reported that ground slope will amplify the soil reaction (Srbulov 2010, Tripe et al. 2013), reduce the soil resistance and decrease the bearing capacity of piles (Choudhury et al. 2006, Van 2014). A recent experimental study by Qu et al. (2020) finds that sloping ground topography may prominently increase the cyclic displacement of single piles.

However, the effects of ground inclination on the dynamic interaction of pile and soil, is still not clear, not to mention the underlying mechanism. On the other hand, the analytical solutions under the irregular boundary conditions, e.g. soil surface inclination (Luco and Mita 1987, Peplow et al. 1999, Qu et al.2017, Ding et al. 2018) are far from sufficient, despite the fact that significant progress in the theoretical aspect has been achieved for pile dynamic analysis (Cui et al. 2018, Li et al. 2019, Luan et al. 2020a, 2020b, Ding et al.2019, Wu et al. 2020). The previous analytical solutions mainly focus on the piles in the ground of horizontal soil profile, which may not adapt to the sloping ground condition. To fill the gaps, this study numerically examines the possible effects on the soil vibration attenuation of free field and the interaction factor of piles in sloping ground. The piles are considered to be end-bearing, and only vertical responses are analyzed, i.e, the larteral deformation of piles are neglected during both the installation and vibration phases (Han et al., 2017, Zhou et al. 2020). Through the amplitude and phase of displacement, sloping ground effects on dynamic pile-to-pile interaction are investigated. Then, a simplified calculating method is proposed on the basis of numerical simulation.

2. Problem definition and method

The problem considered in the current work is the interaction of two cylindrical piles in a sloping ground where one pile is subjected to a vertical dynamic force at the head while the other does not carry any load. The soil is considered as homogeneous, viscoelastic material and

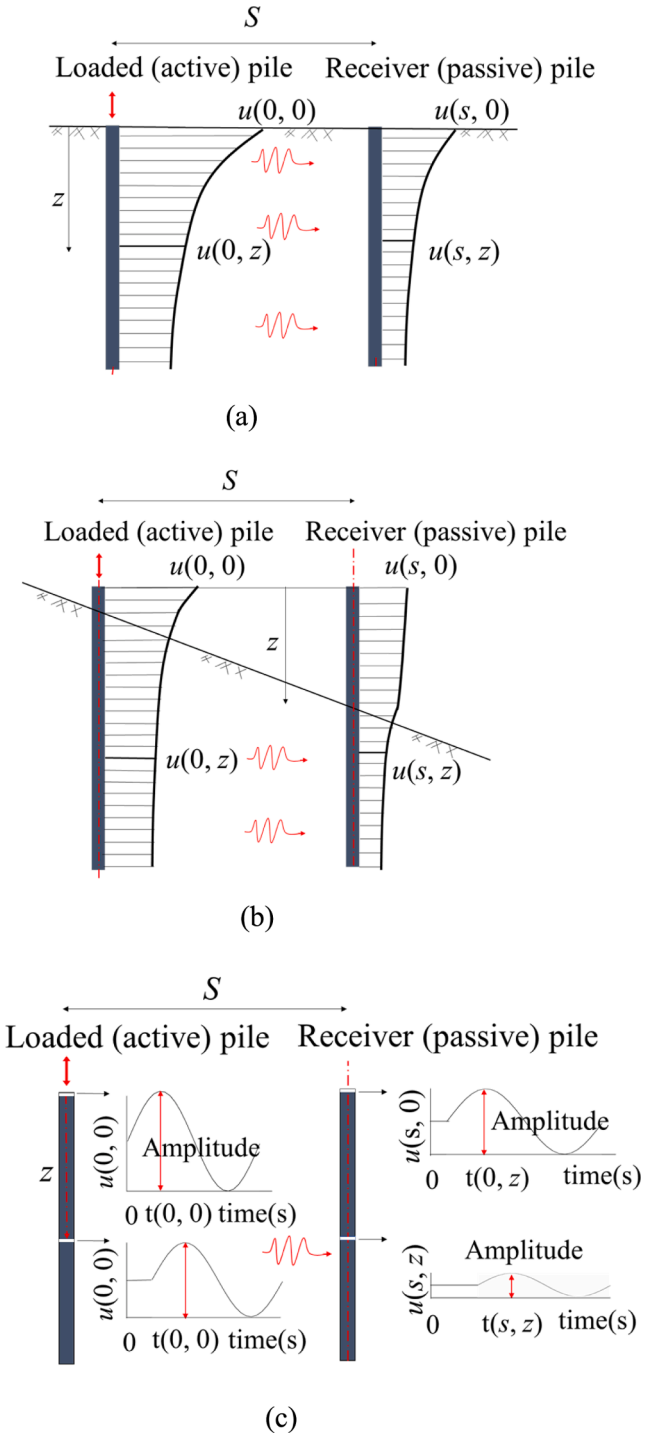

Fig. 2. Schematic illustration of dynamic pile-to-pile interaction in horizontal and sloping ground. (a) Depth profile of vertical displacement amplitudes of a loaded pile and of a passive pile in horizontal ground are assumed to be of the same shape; (b) will the displacement profiles of the two piles in sloping ground remain the same? (c) illustration of amplitude attenuation and time delay in piles.

the pile is assumed to be perfectly elastic; the motion of pile-soil system is assumed to be small and thus no particle breakage (Peng et al., 2021), relative slip and separation (between the pile and soil) could occur during vibration, from those this study's limitation can be derived. Despite of all this, models of such explicit or ideal settings play a fundamental role to understand the nature of complicated dynamic pile soil interaction problem under irregular boundary condition. Fig. 2

Table 1
Soil and pile properties in numerical simulation.

Case ID	Slope angle	Pile length by diameter (H/d)	Embedded pile length by diameter (H_2/d)	Modulus ratio of pile over soil (E_p/E_s)	Number of piles in model
1	0°	15	15	1000	1
2	0°	15	15	100	1
3	0°	30	30	1000	1
4	0°	25	15	1000	1
5	27°	25	15	1000	1
6	45°	25	15	1000	1
7	0°	25	15	1000	3
8	27°	25	15	1000	3
9	45°	25	15	1000	3
10	0°	25	15	100	3
11	27°	25	15	100	3
12	45°	25	15	100	3

shows the dynamic interaction of piles in sloping ground, as well as the horizontal ground that is a natural degradation of that sloping case. For the horizontal ground, it is usually assumed that the shaft perimeter of the loaded pile will simultaneously emit cylindrical waves that propagate horizontally in the radial direction. Under this hypothesis, the vertical displacement amplitude of the active pile and passive pile will share the same profile along depth as shown in Fig. 2**(a)**, and the arriving waves at various depths of the passive pile are all in phase, i.e. no time delay. That deduction is a crucial basis for calculating the dynamic impedance by superposing interaction factors. The reason why the aforementioned approach achieves satisfactory performance for floating piles in homogenous strata, has been shown theoretically (Makris and Gazetas 1993) and numerically (Kanellopoulos and Gazetas 2019). The question arises as to whether the simplified deduction still remain reasonable for end-bearing piles since restrained bottom and pile's rigidity will cause apparent wave diffraction. Moreover, does the displacement profiles of the pile in sloping ground (shown in Fig. 2**(b)**) still obey the aforementioned empirical pattern? And, if not, how does the displacement distribution change? In order to reveal this problem, the amplitude and time delay of the wave crest (shown in Fig. 2**(c)**) in the whole pile-soil system are studied. Harmonic excitation is for conveniently obtaining the amplitude and phase at certain frequencies, which demonstrated an alternative and efficient method (Kanellopoulos and Gazetas 2019) through finite element (FE) method.

3. FE model description and verification

Three-dimensional finite element models developed in this paper are described and verified in this section. In simulation, linear elastic material law is considered for piles and viscoelastic linear material is applied to soil, since non-linear behavior of the soil is often neglected under small strain range (Di Benedetto et al., 2003). The interface between pile and soil is assumed to have perfect contact, i.e, no relative slip and separation occur, which is a common treatment in the domain of dynamic interaction of pile and soil (Kouroussis et al. 2009, Luan et al., 2019, Wu et al., 2020). Dynamic load p considered in this study is vertically distributed on the pile top and has a harmonic wave form of $p = \sin(2\pi ft)$: excitation frequency (f) varies from 0.5 Hz to 10 Hz, which is a common range for soil dynamic analysis. Note that the combined viscous boundary and infinite elements (proposed by Kouroussis et al. 2013), which are capable to provide both stiffness and energy vanish surrounding the finite domain, are introduced to minimize the influence of reflecting waves on the concerned positions: 2d, 5d, 10d radial distance off the pile centerline, where d denotes the pile diameter. Additionally, for the pile medium, only the vertical motion is considered, i.e., the horizontal and bending deformation is suppressed.

The pile characteristics are: mass density ρ_p 2400 kg/m^3; Young's modulus E_p 20 GPa, Poisson's ratio 0.17, diameter d 1 m, shaft length H

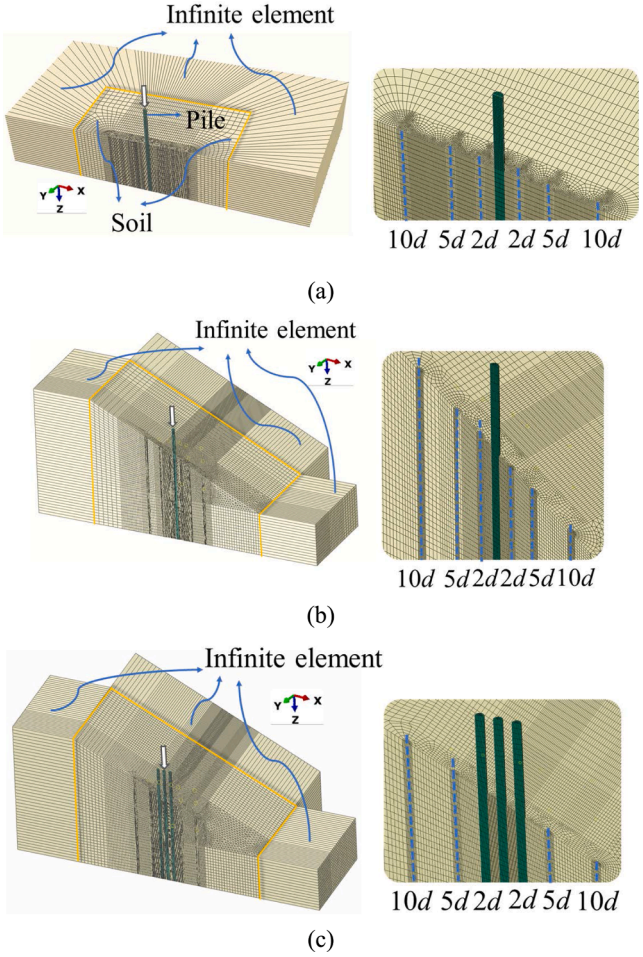

Fig. 3. 3D FE models with various geometry: (a) model for computing soil attenuation factor away from a partially-embedded pile in horizontal ground (case 4); (b) model for computing soil attenuation factor around a partially-embedded pile in sloping ground with angle 27° (case 5); (c) model for computing pile-pile interaction factor at 2d off a partially-embedded pile in sloping ground with angle 27° (case 8).

includes two parts: exposed length H_1 and embedded length H_2; the soil characteristics are: mass density ρ_s 1800 kg/m^3, slope angle $\theta = 0°$, 27° or arctan(0.5), 45°; Young's modulus E_s varies from 20 MPa to 200 MPa; Poisson's ratio 0.3. Detailed parameters of numerical models can be referred Case 1 to Case 12 summarized in Table 1, in which Case 4, Case 5 and Case 8 are presented in Fig. 3**(a), (b) and (c),** respectively. Considering the symmetrical nature of the concerned problem, only half model is built, and the normal direction of symmetry boundary is parallel to Y axis. The meshes around the piles and the zone of interest shown in the right parts of Fig. 3**(a), (b) and (c)**, are modeled using hexahedral solid elements (C3D8 in Abaqus software), and strictly meet the empirical restriction: a maximum element size of $0.1\lambda_{min}$ (Kanellopoulos and Gazetas 2019), where λ_{min} is the minimum concerned wavelength. Rayleigh damping is set to account for the soil damping behavior (Kanellopoulos and Gazetas 2019). The two coefficients α and β of Rayleigh damping can be obtained by: $\alpha = 2\kappa\omega_1\omega_2/(\omega_1 + \omega_2)$, $\beta = 2\kappa/(\omega_1 + \omega_2)$, where α is mass-dependent and β is stiffness-dependent, κ is the damping ratio of soil and a small strain damping level of 5% Rayleigh damping is applied here; ω_1 and ω_2 are the first circular natural frequency and the second natural frequency, respectively, which can be extracted through the Lanczos eigensolver in the frequency module of Abaqus. Iterative algorithm and implicit integration are employed to attain satisfactory accuracy. Dynamic implicit algorithm is carried out in time domain to avoid excessive number of FE

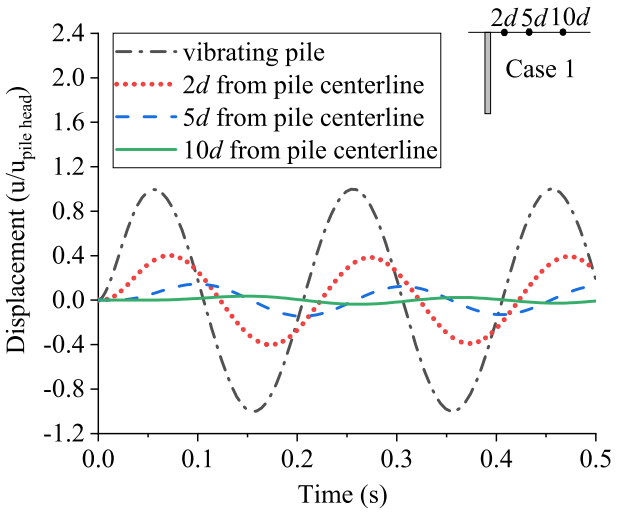

Fig. 4. Vertical displacement time history at different positions of single pile-soil system with a 5 Hz-harmonic excitation at pile head. $H = 15$ m, $d = 1$ m, $E_s = 20$ MPa, $E_p = 20$ GPa.

nodes. (Kouroussis et al. 2009).

Fig. 4 shows the vertical displacement time history at the positions: 0*d* (pile top), 2*d*, 5*d*, 10*d* radial distance from the centerline of the fully embedded pile for Case 1. Obvious time delay and displacement decay are observed when receiver position moves further from the source. In the following analysis, amplitude and phase lag are calculated with the time delay and peak displacement to straightforwardly report the fundamental dynamic behaviors.

To verify the accuracy of the finite element method, the problem of soil vibration attenuation around a single end-bearing pile that is fully-embedded in horizontal ground is considered. The results obtained by the finite element method are compared with a published analytical solution by Luan et al. (2019), which considers the effects of both radially and vertically propagating waves on the soil attenuation factor and gives an accurate solution at low frequency (*f*) range. Natural frequencies of the model can be calculated in Abaqus as $\omega_1 = 10.6$ rad/s, $\omega_2 = 11.8$ rad/s. In order to conform with the study (Luan et al. 2019), the soil damping ratio for verification takes $\kappa = 0.02$. Additionally, alternative calculations that adopt $\kappa = 0.05$ are also done for comparison.

Fig. 5**(a)** shows that the results from FE method at $\xi = 0.02$ well agree with analytical solution in amplitude while the numerically yielded amplitude decreases at high frequency (say larger than 5 Hz in this paper) as κ increases from 0.02 to 0.05. Note that the amplitude at soil is normalized with respect to the one at pile head, i.e, $u(0,0)$, to address the vibration attenuation as frequency varies. Fig.(b) shows that a slight deviation between FE and Luan's solution occurs when *f* exceeds 5 Hz, which is partially due to the different damping settings—hysteretic damping in analytical solution by Luan et al. (2019) and Rayleigh damping in the presented FE model. It reflects that the Rayleigh damping, to some extent, overestimates the phase at high frequency because of indirect approximation of physical energy dissipation (Kramer 1996). Whereas, the numerical algorithm demonstrates a feasible technique to deal with the wave propagation problem.

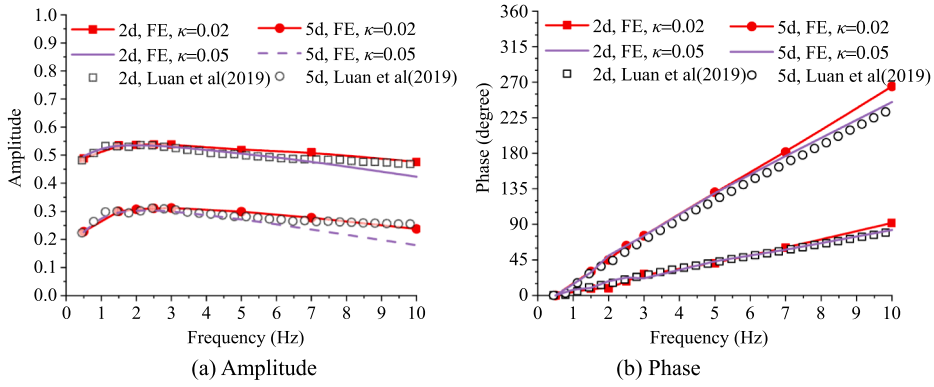

Fig. 5. Comparisons of soil attenuation factors between the used finite element and available analytical solution for horizontal ground. $E_p = 25$ GPa, $E_s = 26$ MPa, $H = 20$ m; $d = 1$ m.

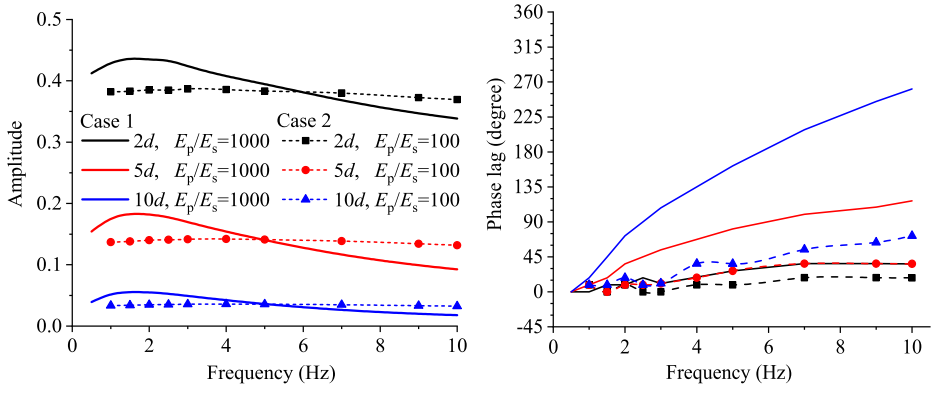

Fig. 6. The influences of critical parameters of pile-soil system on the soil attenuation factor in level ground ($H/d = 15$). Amplitudes at 2*d*, 5*d*, 10*d* soil positions are normalized with respect to the one at pile head.

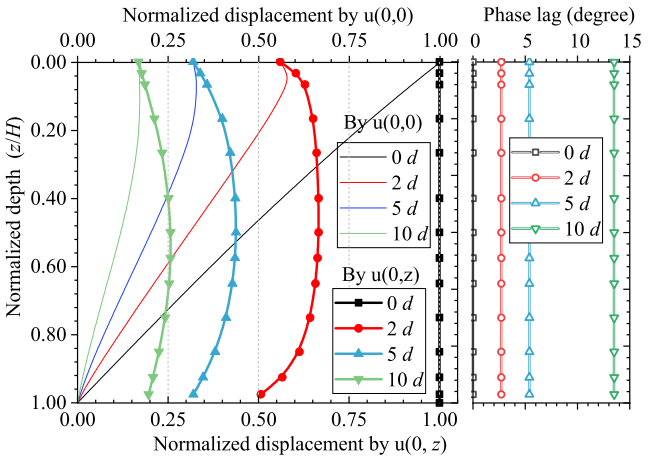

Fig. 7. Normalized displacement profile of single-pile system at frequency 0.5 Hz for Case 3.

4. Dynamic interaction of soil and pile in horizontal ground

4.1. Soil vibration attenuation around fully embedded pile

The soil deformation tends to decrease as the wave spreads out. In this section, vibration characteristics of pile in horizontal ground is presented to capture the main features of dynamic pile-soil interaction in horizontal ground.

Cylindrical wave type is an empirical but robust rule that estimates the soil vibration induced by a vertically floating pile in level ground, which premises on the assumption that the compressive wave along vertical direction is neglectable. The natural frequency of soil deposit can be estimate by the formula $f = V_s/4H$, in which V_s denotes shear wave speed in soil. Therefore, the values of natural frequency for Case 1 and Case 2 gets 1.1 Hz and 3.4 Hz. Fig. 6 shows the influence of pile-soil relative stiffness (E_p/E_s) on the displacement of soil surface at various positions at various loading frequencies. In Fig. 6**(a)**, it is observed that the amplitude notably decays when the receiving positions moves away from pile centerline. Nonetheless, the influence of relative stiffness on the displacement amplitude is not significant. For $E_p/E_s = 1000$, a similar frequency-dependent attenuation amplitude is observed on the curves for 2*d*, 5*d* and 10*d* from pile axis: The amplitude for soil attenuation factor increases to maximum at less than 1.5 Hz, and then gradually falls in Fig. 6**(a)**. For $E_p/E_s = 100$, it appears that the amplitude of soil peaks at around 4 Hz whereas it is generally insensitive to frequency. The explanation for the different behaviors on stiff soil ($E_p/E_s = 100$) and soft soil ($E_p/E_s = 1000$) is straightforward: waves in stiff soil tend to spread in three dimensions (compressive wave components emerge) and thus exhibit more rapid decay in amplitude at low frequency range; on the other hand, waves in stiff soil travel with greater speed, which leads to the obvious reduction of phase lag as E_p/E_s decreases from 1000 to 100. Also, energy loss in soft soil significantly increases with frequency whereas that growth for stiff soil is gently mild as indicated in Fig. 6**(b)**, which accounts for the trend that amplitude for $E_p/E_s = 100$ remains larger than that for $E_p/E_s = 1000$ at larger frequency range.

The displacement along depth plays a role in revealing how soil deforms and how waves propagate inside the pile-soil system. **In** Fig. 7 (left), the single solid line and solid line with symbol show the displacement normalized by the pile top displacement $u(0,0)$, and the one normalized by the pile shaft displacement at the same horizontal $u(0,z)$, respectively. Note that the considered loading frequency is 0.5 Hz. It is found that the displacement at pile centerline constantly falls as pile depth increases. However, for the soil displacement along 2*d* centerline, the displacement reduces slowly within a certain depth, then quickly decreases till zero. That critical depth tends to increase when receiver positions moves away from the pile centerline. On the other hand, when the displacement along depth is normalized by shaft displacement of the loaded pile, it is found that the displacement varies a little along depth, which indicates the soil displacement attenuation is relatively stable along depth. The right part of Fig. 7 shows that the phase lag gradually increases as radial distance increases (the same hereinafter). At $f = 0.5$ Hz, the phase is less than 15° for a range of 10*d* radial distance and is nearly invariable along depth.

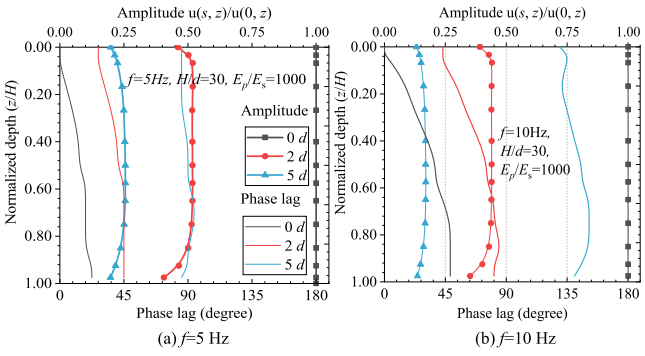

Fig. 8. Depth profiles of amplitude and phase lag at various frequencies for Case 3.

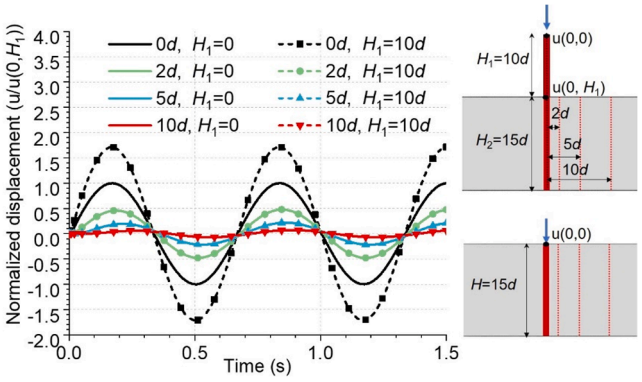

Fig. 9. Comparisons of time-domain displacements in partially and fully embedded pile-soil system. $f = 0.5$ Hz for Case 1 and Case 4.

Following the similar method, the normalized amplitude and phase lag at 2*d*, 5*d* radial distance are shown at $f = 5$ Hz, $f = 10$ Hz in Fig. 8**(a) and (b)** respectively. It is evident that the normalized amplitude becomes flatter as frequency increases. Another finding is that the phase lag along depth significantly increases with increasing frequency-the phase lag at different depth of pile can rise to near 50° at 10 Hz. Thus, for end-bearing piles, the typical assumption by Dobry and Gazeta (1988) that the out-going waves emit simultaneously from all the perimetric points of pile shaft may cause unneglectable deviation as frequency grows. Nevertheless, at $E_p/E_s = 1000$, the phase difference among different radial distances (0*d*, 2*d*, 5*d*) vary rather limitedly as depth increases, which justifies the simplification by Mylonakis et al. (1998) that the shear waves generated from pile shaft propagates in approximately horizontal manner.

4.2. Influence of exposed pile segment on soil vibration attenuation

The vibration energy in the unembedded pile segment relies on the mass and loading frequency and will naturally affect the displacement in the embedded one. It remains not yet sure whether the exposed segment plays a role in the dynamic pile soil interaction. Fig. 9 compares the time-domain displacements between a partially and a fully embedded pile, including pile head displacements denoted by $u(0, 0)$ or 0*d* and soil displacements at 2*d*, 5*d* and 10*d* radial distances. Note that the

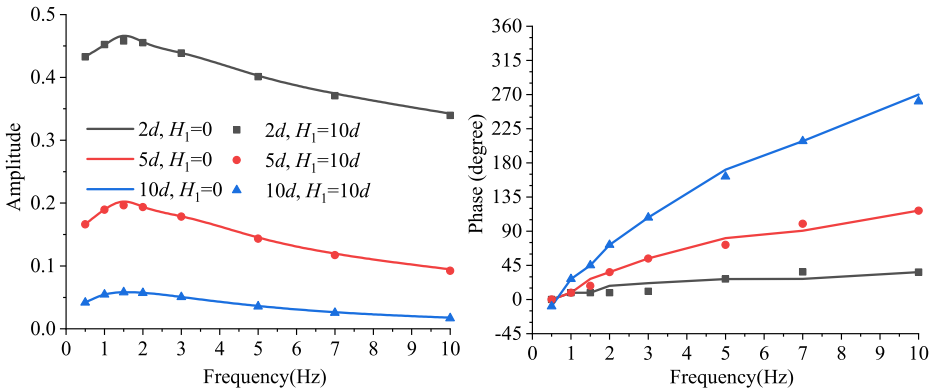

Fig. 10. Comparison of soil attenuation factor between partially and fully embedded piles. Amplitudes at 2*d*, 5*d*, 10*d* are normalized with respect to the one of pile section at ground level.

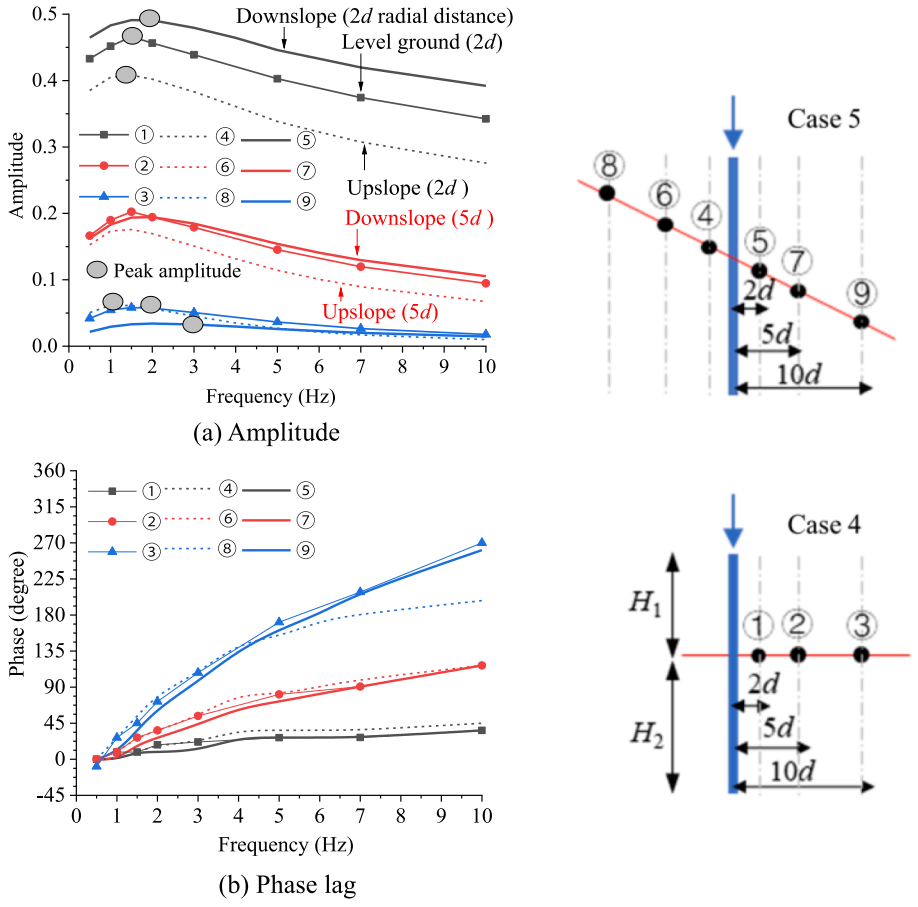

Fig. 11. Comparison of soil attenuation factors along two directions in sloping ground and horizontal ground. $Ep/Es = 1000$, $H_1 = 10d$, $H_2 = 15d$, slope angle 27°.

displacements here are normalized by the pile displacement of the partially embedded pile at the embedded level, namely by $u(0, H_1)$. It is apparently that the additional free length amplifies the displacement at pile top but barely modifies the soil displacement.

Furthermore, Fig. 10 shows that the exposed segment hardly changes the soil attenuation factor (both amplitude and phase) at given frequencies. It is anticipated because that the apparent velocity of compression-extension wave in a free bar approximates the longitudinal wave speed, and thus the time delay and amplitude decay are rather small when the wave passes through the exposed segment. Hence the influence of exposed segment will not be further discussed in this study.

5. Vibration attenuation and wave propagation in sloping ground

5.1. Direction-dependent soil attenuation factor on sloping ground

Vibration attenuation of soil relies on the pile-soil interaction and wave propagation manner. As shown in Fig. 11**(a)**, the soil attenuation factor in sloping ground, which is calculated using the pile head displacement, is direction-dependent: upslope amplitude is generally smaller than downslope, which arises from the different geometric damping and energy dispersion when waves pass through downslope and upslope. Furthermore, the amplitude varies with the receiving

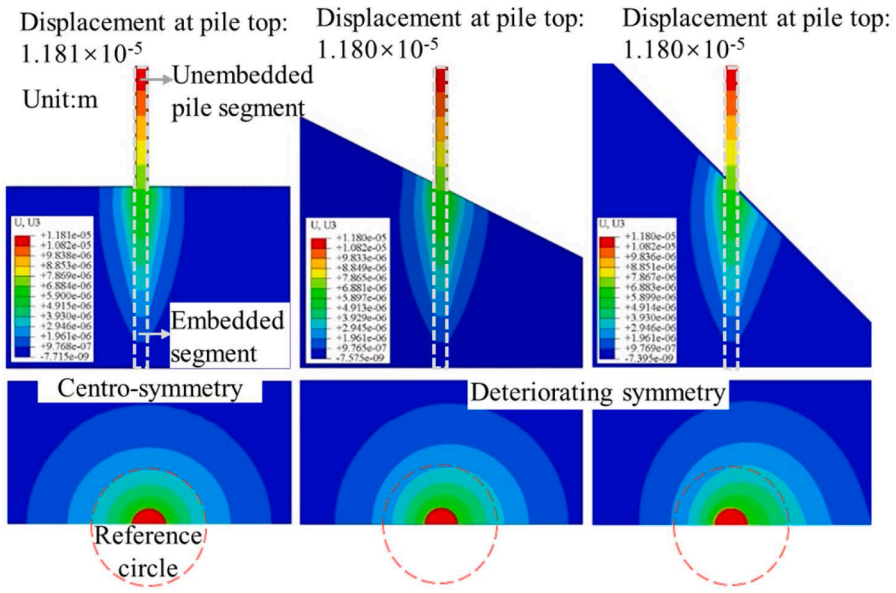

Fig. 12. Peak displacement contours of soil-pile systems under various ground inclination. $E_p/E_s = 1000$, $H = 25d$, $H_1{:}H_2 = 2{:}3$, $f = 5$ Hz; the centers of reference circles locate at the pile centerlines.

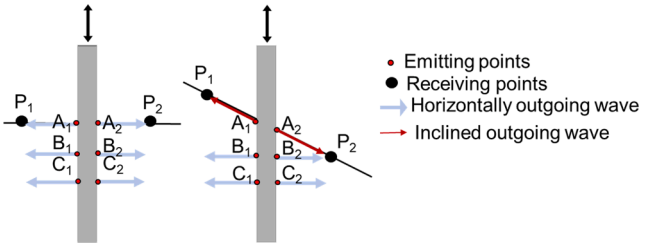

Fig. 13. The wave propagation paths of vibrating pile in horizontal and sloping ground.

position. The amplitude in horizontal ground is taken as reference. At 2*d* off loaded pile, the reference amplitude is between upslope and downslope; at 5*d* and 10*d*, it approaches to the value on downslope. Besides, the peak frequency seems to be dependent with the deposit height at receiving position, which is understandable since resonant frequency of soil field is positively correlated with soil height from sub rock (Gutowski et al. 1976). As shown in Fig. 11**(b)**, the phases among different topography generally have small differences except that upslope 10*d* position yields obvious phase lag when frequency exceeds 5 Hz, which may be attributed to the large soil damping along upslope. Considering that the vibration at 10*d* position is quite weak, the phase lag can only exert an insignificant influence on interaction. Therefore, the displacement amplitude is exclusively focused in the hereafter analysis.

The graphical comparison of vertical displacement field, shown in Fig. 12, can reveal what happens for the vibrating pile-soil system when the wave spread out along sloping ground. It is clear that the displacement of the loaded pile is rather insensitive to ground inclination. For the soil domain, perfectly central symmetry is observed for the displacement contours in the case of horizontal ground. However, the symmetry tends to deteriorate when slope angle increases. It is observed that the displacement concurs tend to deviate with the reference circles as slope increases. Also observe that the wave front near ground surface obviously tilts (approximately parallel to the ground surface) when wave propagates upslope; while only limited wave rays change paths

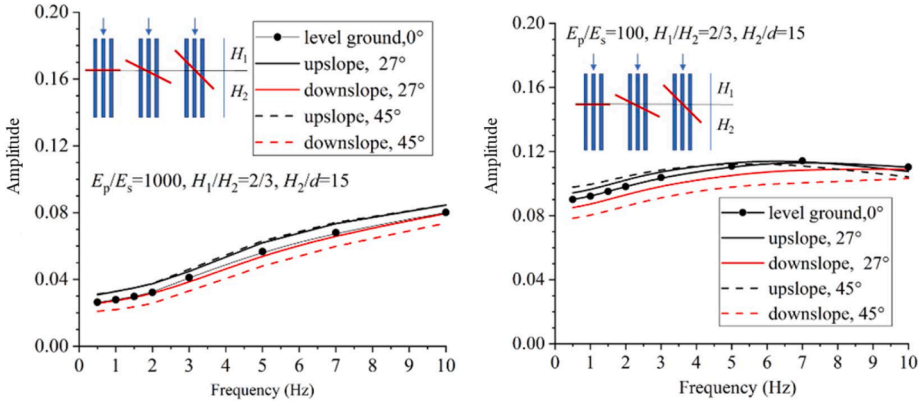

(a) E_p/E_s=1000 (Case 7, 8, 9) (b) E_p/E_s =100 (Case 10, 11, 12)

Fig. 14. Sloping ground effects on interaction factor with frequency variation for the pile-soil system with different properties. $H_1/H_2 = 2/3$, $H_2/d = 15$.

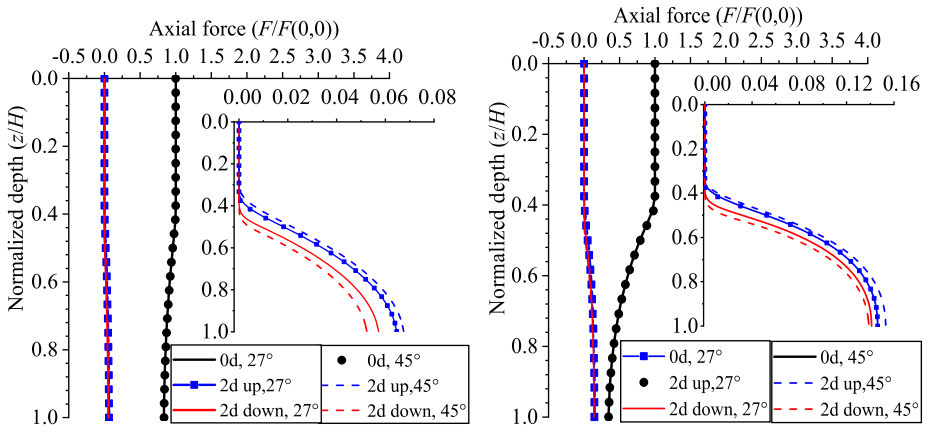

(a) E_p/E_s =1000 (Case 7, 8, 9) (b) E_p/E_s =100 (Case 10, 11, 12)

Fig. 15. Sloping ground effects on axial force profile. $H_1/H_2 = 2/3$, $H_2/d = 15$, $f = 0.5$ Hz.

through downslope.

The wave paths (similar with the concept of 'wave rays' in Gazetas and Makris, 1991) illustrated in Fig. 13 may explain the differential vibration of soil field located downslope and upslope. Just consider the case of $E_p/E_s = 1000$ or larger in horizontal ground, Section 3.1 has confirmed that horizontal wave dominates the soil vibration at that condition, which is shown in the left sketch in Fig. 13. By contrast, for the case of sloping ground, no horizontal wave from vibrating pile can directly reach P_1, thus the vibration of P_1 in sloping ground is impaired because of lacking a significant portion of energy. At the same time, P_2 receives supplementary energy from inclined waves and thus vibrates a little bit more dramatically compared with P_2 in horizontal ground.

5.2. Interaction factors in sloping ground

Fig. 14(a) shows that the interaction factor of receiver pile increases with frequency at similar increasing rates for different ground inclinations at $E_p/E_s = 1000$. Moreover, the pile positioned upslope obtains the larger interaction factor. The divergence between upslope pile and downslope pile increases from around 20% to 40% as the slope increases from 27° to 45°. Note that frequency appears to exert a weak influence on that divergence. In addition, when the slope is milder (27°in this study), the pile located downslope suffers approximate vibration with horizontal ground, which indicates that the downslope pile is less affected under gentle slope topography. At E_p/E_s 100 and buried length $H_2 = 15d$, the interaction factor becomes flatter as depicted in Fig. 14 (b). Moreover, divergence between upslope and downslope piles shows a decreasing trend as frequency increases; and no significant difference is observed at 10 Hz.

Fig. 15 shows the variation of axial force profile for the piles in the ground of various inclination. It is obvious that the axial force gradually reduces after the loaded pile is buried in the soil. As for the passive piles, the axial force of free segment approaches zero, and it increases with the buried length at a decreasing rate. Furthermore, larger axial force is observed in the passive pile at upslope side, which reflects that the pile with longer frictional length receives larger energy from the near vibrating soil.

6. Simplified solution to sloping effects

6.1. Solving process

The pile-to-pile interaction process includes three stages: (1) an oscillating pile exerts shear force to surrounding soil by friction; (2) wave propagates into the soil and cause soil vibration; (3) the passive pile is stroked by the arriving spreading waves and starts to vibrate. In sloping ground, piles that are embedded in different locations have different friction lengths between pile and soil, which causes various pile responses. As shown in Fig. 16, the interaction factors are calculated in two directions: downslope and upslope. The lateral soil resistance is

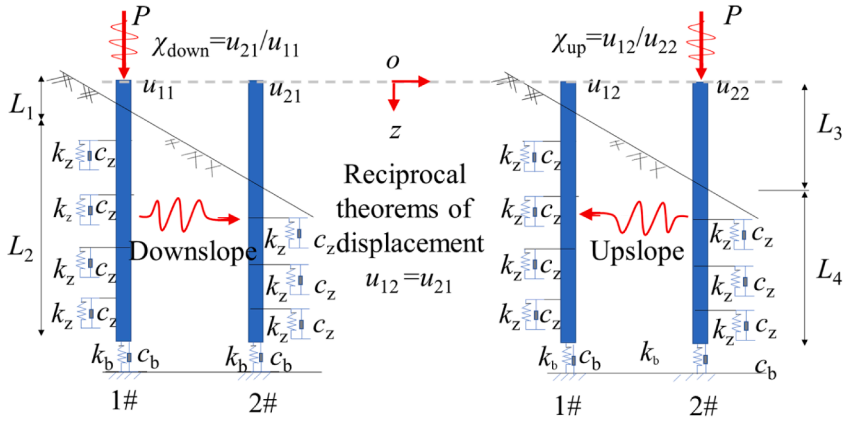

(a) wave propagates towards downslope (b) wave propagates towards upslope

Fig. 16. Calculation model for the dynamic interaction factor of the piles in slope ground.

simplified as a series of vertical springs and viscous dampers with the coefficients k_z and c_z, respectively—for the bottom soil, those are k_p and c_p. Then, the intended downslope interaction factor χ_{down} can be expressed as the displacement ratio u_{21}/u_{11} and upslope interaction factor $\chi_{up} = u_{12}/u_{22}$, in which the top vertical displacement u_{21} of downslope passive pile 2# equals u_{12} of upslope passive pile-—application of the reciprocal theorems of displacement.

On the basis of the conclusions in the Section 4.2, Section 5.1 and Section 5.2, following assumptions can be proposed to simplify the problem: (1) the influence of unembedded pile segment on the pile-pile interaction factor could be ignored; (2) the waves towards the downslope mainly spread radially. Therefore, the interaction factor $\alpha_v(s)$ of the embedded pile segment could be written as:

$$\alpha_v(s) = \varphi\xi \tag{1}$$

where φ is the soil attenuation factor of the free field, and ξ is the diffraction factor that is proposed to account for the diffraction effect of the arriving waves in the presence of receiver pile (Mylonakis and Gazetas, 1998):

$$\varphi(s) = \frac{H_0^2\left(\frac{s}{d}\frac{a_0}{\sqrt{1+2i\kappa}}\right)}{H_0^2\left(\frac{1}{2}\frac{a_0}{\sqrt{1+2i\kappa}}\right)} \tag{2}$$

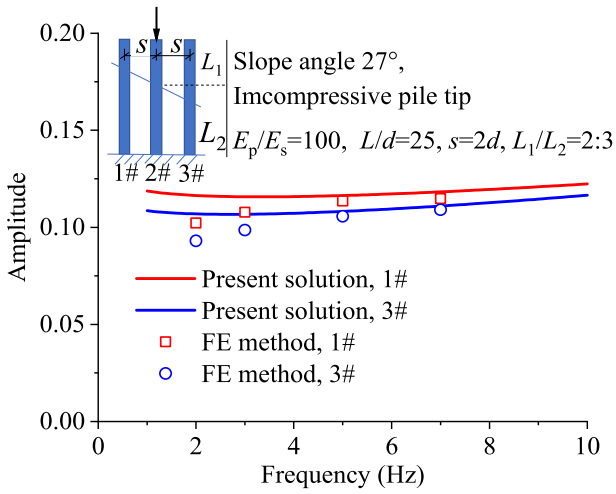

Fig. 17. Comparisons between the simplified solution and FE numerical results for the interaction factors in sloping ground.

Hence, the displacement of the passive pile at the ground horizontal on downslope direction can be expressed as:

$$u_3(L_3) = u_3(0)cos\left(\frac{\omega}{C_p}L_3\right) \tag{8}$$

$$\xi(s) = \frac{\widetilde{k}}{\left(\widetilde{k} - \rho_p A_p \omega^2\right)} \frac{2L_4\frac{\lambda}{C_p} + sinh\left(2L_4\frac{\lambda}{C_p}\right) + \left(\frac{k_b C_p}{E_p A_p \lambda}\right)^2\left[sinh\left(2L_4\frac{\lambda}{C_p}\right) - 2L_4\frac{\lambda}{C_p}\right] + 2\frac{k_b C_p}{E_p A_p \lambda}\left[cosh\left(2L_4\frac{\lambda}{C_p}\right) - 1\right]}{2sinh\left(2L_4\frac{\lambda}{C_p}\right) + 2\left(\frac{k_b C_p}{E_p A_p \lambda}\right)^2 sinh\left(2L_4\frac{\lambda}{C_p}\right) + 4\frac{k_b C_p}{E_p A_p \lambda}cosh\left(2L_4\frac{\lambda}{C_p}\right)} \tag{3}$$

where s is the axis-to-axis spacing; a_0 is non-dimensional frequency and equals $\omega d/V_s$; ω is the circular frequency, is the soil damping ratio; V_s is the shear wave velocity of soil; L_4 denotes the embedded length of the passive pile; ρ_p, A_p, d are the mass density, cross section area and diameter of the pile, respectively; $\widetilde{k}$ is the elementary soil resistance that takes $\widetilde{k} = k_z + ic_z$; $\lambda = \sqrt{\omega^2 - \widetilde{k}/\rho_p A_p}$; k_b and c_b represent the soil resistances at pile tip, which can be refered Gazetas et al. (1991). Specially, when the soil at pile tip is incompressive, $k_b \to \infty$ and Eq. (3) can be simplified as:

$$\xi(s) = \frac{\widetilde{k}}{2\left(\widetilde{k} - \rho_p A_p \omega^2\right)}\left[1 - \frac{2L_4\sqrt{\frac{\widetilde{k} - \rho_p A_p \omega^2}{E_p A_p}}}{sinh\left(2L_4\sqrt{\frac{\widetilde{k} - \rho_p A_p \omega^2}{E_p A_p}}\right)}\right] \tag{4}$$

The general solution to the displacement and axial force of the unembedded segment of the passive pile can be written as:

$$u_3(z) = A_3 cos\left(\frac{\omega}{C_p}z\right) + B_3 sin\left(\frac{\omega}{C_p}z\right) \tag{5}$$

$$N_3(z) = -E_p A_p \frac{\omega}{C_p}\left[-A_3 sin\left(\frac{\omega}{C_p}z\right) + B_3 cos\left(\frac{\omega}{C_p}z\right)\right] \tag{6}$$

Combining the initial condition and boundary condition, one can obtain:

$$A_3 = u_3(0); B_3 = 0 \tag{7}$$

Assuming the head displacement of the active pile as one, then the load at pile top of the active pile is $z(0)$, and thus the displacement of active pile at ground horizontal can be written as:

$$u_1(L_1) = cos\left(\frac{\omega}{C_p}L_1\right) + \frac{\frac{\lambda\psi}{\omega} + tan\left(\frac{\omega}{C_p}L_1\right)}{1 - \frac{\lambda\psi}{\omega}tan\left(\frac{\omega}{C_p}L_1\right)} sin\left(\frac{\omega}{C_p}L_1\right) \tag{9}$$

the displacement of passive pile at ground horizontal is expressed as:

$$u_3(L_1) = \alpha_v(s)\left[cos\left(\frac{\omega}{C_p}L_1\right) + \frac{sin\left(\frac{\omega}{C_p}L_1\right)}{A_1/B_1}\right] \tag{10}$$

where the coefficient of A_1/B_1 can be calculated by Eq. A15.

One can obtain the pile-to-pile interaction factor on downslope:

$$\chi_{down} = \alpha_v(s)\left[\cos\left(\frac{\omega}{C_p}L_1\right) + \frac{\sin\left(\frac{\omega}{C_p}L_1\right)}{A_1/B_1}\right] \Big/ \cos\left(\frac{\omega}{C_p}L_3\right) \tag{11}$$

The reciprocal theorem is performed to establish the relationship between the interaction factor on upslope χ_{up} and the one on downslope χ_{down}. As illustrated in Fig. 15, assume the load P as a unit force, then the vertical displacement of the piles can be written:

$$u_{11} = 1/Z_1(0) \tag{12}$$

$$u_{21} = \chi_{down}/Z_1(0) \tag{13}$$

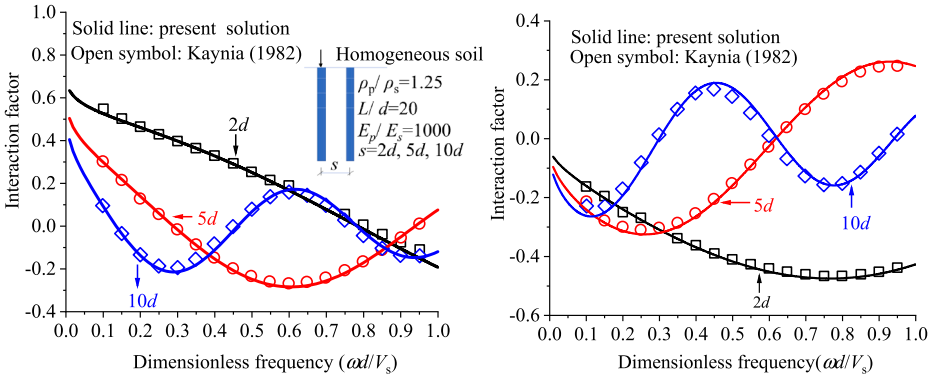

Fig. 18. Verification of the present solution for the interaction factor in horizontal ground.

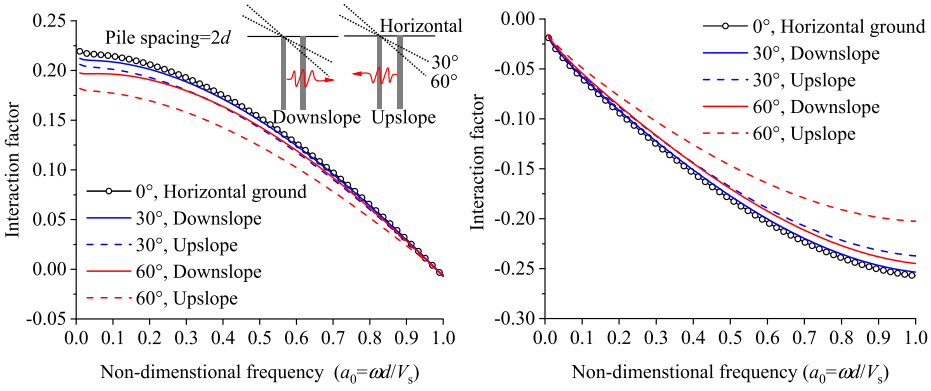

Fig. 19. Frequency-dependent dynamic interaction factors in sloping ground; $s = 2d$; $L/d = 40$; $E_p/E_s = 1000$.

$$u_{22} = 1/Z_2(0) \tag{14}$$

where $Z_1(0)$ is the dynamic impedance at the top surface of the upslope pile 1#; $Z_2(0)$ is the dynamic impedance at the top of the downslope pile 2#, which can be caluculated by Eq. A16

The reciprocal theorem is given by:

$$u_{12} = u_{21} \tag{15}$$

Combined with the Eq. (13), Eq. (14) and Eq. (15), the pile-to-pile interaction factor towards upslope can be formulated as:

$$\chi_{up} = \frac{u_{12}}{u_{22}} = \chi_{down}\frac{Z_2(0)}{Z_1(0)} \tag{16}$$

6.2. Comparison and verification

First, we compare the interaction factors in sloping ground obtained by the present solution and FE method in Fig. 17. The results show that the amplitude calculated by present solution is slightly larger than that by FE method in low frequency range (e.g., 2 Hz, 3 Hz), which reflects that neglecting longitudinal waves in soil field may overestimate, to

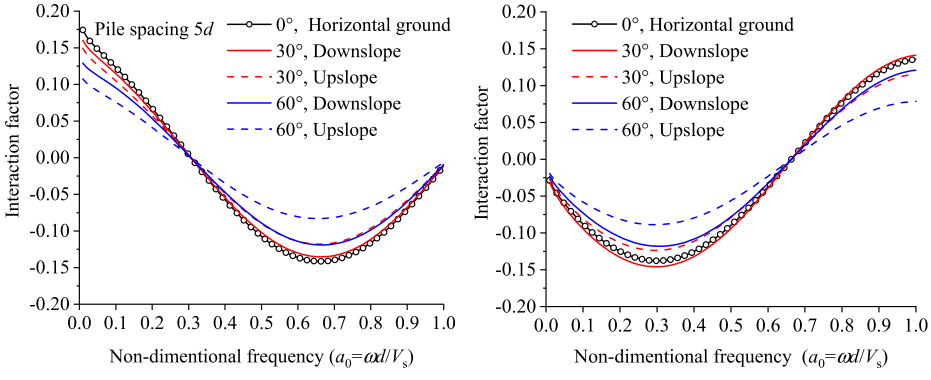

Fig. 20. Frequency-dependent dynamic interaction factors in sloping ground; $s = 5d$; $L/d = 40$; $E_p/E_s = 1000$.

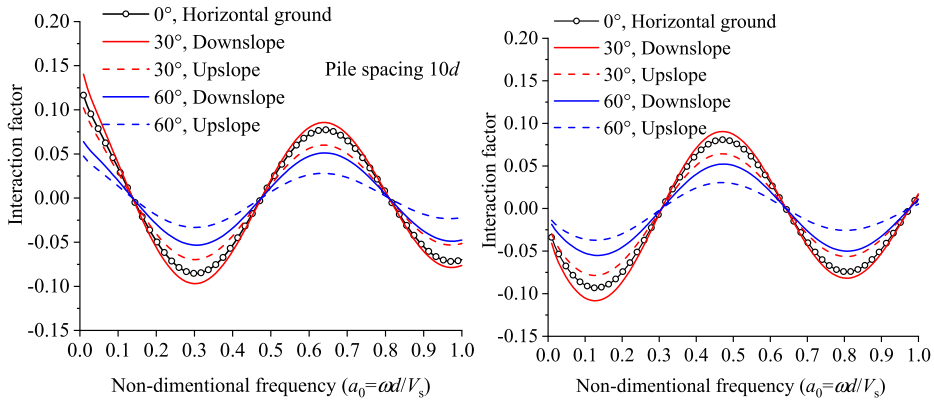

Fig. 21. Frequency-dependent dynamic interaction factors in sloping ground; $s = 10d$; $L/d = 40$; $E_p/E_s = 1000$.

some extent, the interaction between pile and soil at low frequency. As frequency increases, the present solution produces satisfactory accuracy.

On the other hand, note that dynamic interaction factor is essentially a complex number, which can be constituted by amplitude and phase or alternatively by the real part and imaginary part. The latter form of constitution often used to reveal the mechanical performance and energy dissipation, whereas the former reflects the basic characteristics of waveform. From the practical perspective, we hereafter adopt the latter form of interaction factor for dynamic analysis. Eq. (15) degenerates into $\chi_{up} = \chi_{down}$ when $L_1 = L_3 = 0$, which represents the interaction factors in horizontal ground. In Fig. 18, the presented solution is compared with the study by Kaynia and Kausel (1982) that is based on the boundary element method and is considered an accurate solution for interaction factors of piles in horizontal ground. The results show that both the real and imaginary components based on this presented solution agree with that in Kaynia and Kausel (1982), which proves the efficacy of the present solution at the extreme condition of 0° slope.

7. The sloping effects on dynamic response of group of piles

7.1. Sloping effects on pile-to-pile interaction

The parameters are: pile slender ratio $L/d = 40$, pile spacing $s = 2d$, $5d$, $10d$. Young's modulus, mass density of pile and soil are, $E_p/E_s = 1000$, $\rho_p/\rho_s = 1.33$; Poisson's ratio υ and damping ratio of soil are = 0.3, $\zeta = 0.05$. Slope effects are dependent on the inclination angle of the ground and the location of the passive pile. The results in Fig. 19, Fig. 20, **and** Fig. 21, which are calculated with the presented analytical solution, show the variation of pile-to-pile interaction factor with frequency when the vibration propagates downslope and upslope at various slope angles at pile spacing $2d$, $5d$, $10d$ respectively. In general, to what extent the ground inclination exerts influence is closely related with the frequency and is not linear variation with the slope angle.

In Fig. 19, it is observed that varying slope angles lead to prominent deviation at the low frequency for the real part of interaction factor. As frequency increases, the topography effects on the real part tend to become weaker. At pile spacing $s = 2d$, the interaction factor that induced by the waves towards slope crest is evidently smaller than the one that induced by the waves towards slope toe, and that difference increases with the slope angle—around 25% smaller for 60° slope angle in Fig. 19**(a)**. A converse frequency dependency is observed for the imaginary part of the interaction factor shown in in Fig. 19**(b)**.

Combined with the results in Fig. 20 and Fig. 21, it is found that the slope effects become more complicated as pile spacing increases. The curves of interaction factor versus frequency meet identical crossing points for different slope angles. In Fig. 20**(a)**, the intersection frequencies are around $a_0 = 0.3$ and $a_0 = 1.0$. Before $a_0 < 0.3$, the slope effects on the interaction factor becomes weaker with increasing frequency. Moreover, the interaction factor toward downslope is larger than the one towards upslope. As the value of a_0 ranges from 0.3 to 1.0, slope effects intensify at the beginning, come to a peak around $a_0 = 0.65$, then gradually become weaker on the way to $a_0 = 1.0$. Furthermore, the similar crossing point around $a_0 = 0.6$ is observed for the imaginary part in Fig. 20**(b)**. The topography effects on the imaginary part is also similar to the real part. In Fig. 21, three crossing points occur, and their frequency intervals are around 0.3.

Our results in Fig. 19, Fig. 20, Fig. 21 confirm that ground inclination exerts undisputable influences on the dynamic interaction factor. Generally, it will reduce the peak value of interaction factor and weaken the fluctuation with frequency. The reduction by the sloping ground sometimes exceeds 20%, which means that neglecting sloping effects will bring in a considerable overestimation to the pile-to-pile dynamic interaction.

7.2. Dynamic impedance of group piles in sloping ground

The group of piles herein are considered to be connected with a no-mass rigid cap. Harmonic excitation is vertically applied on the cap. Therefore, the vertical displacement of the cap is identical with all the beneath piles, which yields:

$$u_G \frac{E_p A_p}{L} = \sum_{j=1}^{n} \frac{\chi_{ij}}{\frac{\widetilde{Z}_j L}{E_p A_p}} p_j = \sum_{j=1}^{n} \beta_{ij} p_j \tag{35}$$

where u_G is the vertical displacement of the cap; E_p, A_p, L are the Young's modulus, cross section area, and length of piles, respectively; P_j is the load acting on the j pile head; $\widetilde{Z}_j$ is the dynamic impedance of j pile at head; χ_{ij} $(i, j = 1, 2, \ldots n)$ is the dynamic interaction factor between j pile and i pile; the coefficient β_{ij} can be calculated as following:

$$\beta_{ij} = \frac{\chi_{ij}}{\frac{k_j L}{E_p A_p}} \tag{36}$$

The external load P is simultaneously taken by all the piles:

$$P_G = \sum_{j=1}^{n} P_j \tag{37}$$

Combined with Eq. (35) and Eq. (37), the vertical displacement u_G of the capped piles and the load P_j undertaken by pile j can be given by solving the following matrix equation:

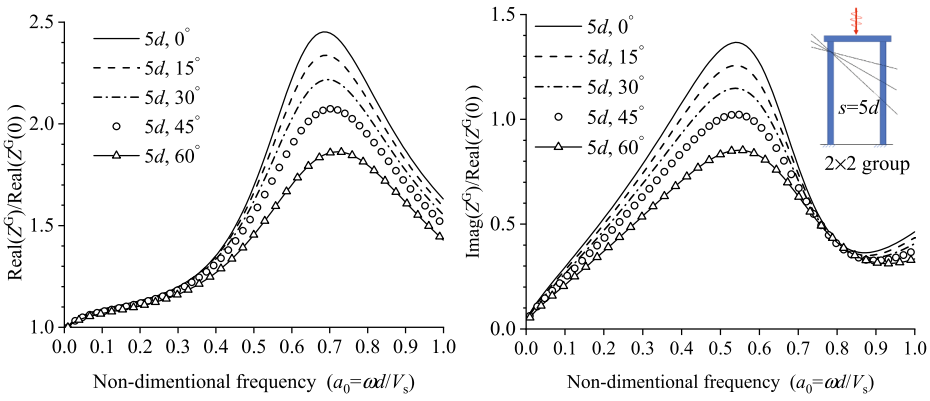

(a) Real part (b) Imaginary part

Fig. 22. Dynamic impedance factors of group of piles at various slopes ($L = 40d$, $s = 5d$).

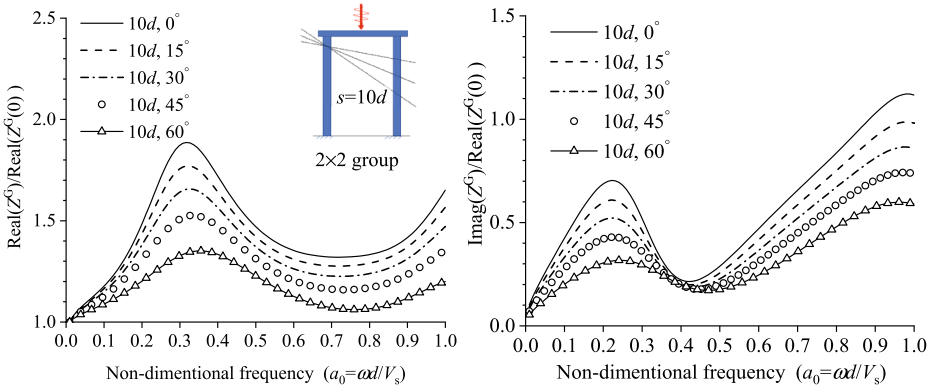

(a) Real part (b) Imaginary part

Fig. 23. Dynamic impedance factors of group of piles at various slopes ($L = 40d$, $s = 10d$).

$$\begin{bmatrix} 0 & 1 & 1 & \dots & 1 \\ -1 & \beta_{11} & \beta_{12} & \dots & \beta_{1n} \\ -1 & \beta_{21} & 1 & \dots & \beta_{2n} \\ \dots & \dots & \dots & \dots & \dots \\ -1 & \beta_{n1} & \beta_{n2} & \dots & \beta_{nn} \end{bmatrix} \begin{Bmatrix} u_G \frac{E_p A_p}{L} \\ P_1 \\ P_2 \\ \dots \\ P_n \end{Bmatrix} = \begin{Bmatrix} P \\ 0 \\ 0 \\ \dots \\ 0 \end{Bmatrix} \tag{38}$$

Therefore, the dynamic impedance of the group of piles in sloping ground can be expressed by:

$$Z^G = P/u_G \tag{39}$$

The notable difference induced by ground inclination lies in the fact that $\beta_{ij} \neq \beta_{ji}$, which indicates that the coefficient matrix in Eq. (38) is not symmetric. To clearly observe the dynamic impedance variation with frequency, the concept of dynamic impedance factor (DIF) is introduced by dividing the dynamic impedance by the static stiffness (approach with the real part of dynamic impedance at zero frequency). The results in Fig. 22 and Fig. 23, which are calculated with the presented analytical solution, show the variation of DIF with frequency on various slope angles at pile spacing $s = 5d$ and $10d$, respectively. In Fig. 22**(a)**, it is observed that DIF peaks at some frequency range $0.4 < a_0 < 0.8$. At $a_0 < 0.4$, ground inclination exerts disposable influence on the real part of DIF; after that, the real part of DIF of piles in the grounds of various slope angles starts to diverge with the frequency, and the greatest difference occurs at the peak frequency. The steeper the slope is, the larger the peak frequency becomes, and the smaller the peak DIF gets. To be specific, the real part of DIF at slope angle 60° is reduced by 25% than that in horizontal ground. Similar characteristics could be found for the curves of dynamic damping versus frequency as shown in Fig. 22**(b)**: topography effects tend to get intense before the peak frequency and get weaker after the peak frequency. At pile spacing $10d$, the dynamic stiffness gradually diverges from the very low frequency (around zero) and peaks at a smaller frequency (approximately half) than that at pile spacing $s = 5d$. Generally, increasing the pile spacing causes more significant topography difference in the dynamic impedance, especially in the dynamic damping. The reduction of dynamic stiffness and dynamic damping are around 30% and 50%, respectively compared with that in horizontal ground.

8. Conclusions

Dynamic interaction between pile and soil in sloping ground are explored via finite element-based simulations. The wave propagation process, vibration attenuation of a free field, and displacement of passive piles are numerically investigated. Additionally, on the basis of the numerical research, an analytical model is built to obtain the vertical pile-to-pile interaction factors. A comparison between the analytical solution and the numerical results confirms the rationality of the present model. Subsequently, dynamic responses of group piles in sloping ground are studied through the superposition method. The following conclusions can be drawn:

(1) The soil attenuation factor in sloping ground is direction-dependent: the position at the downslope from pile axis suffers greater vibration than the one at the upslope.

(2) The piles in sloping ground have unequal embedded lengths and thus the stiffness of each individual pile is different from one another, which is the leading factor affecting the dynamic pile-to-pile interaction in sloping ground.
(3) Ground slope mainly has twofold effects on the pile-to-pile interaction: (a) direction dependency: the interaction factor induced by the waves towards slope toe is slightly smaller than the one towards slope crest; (b) inclination angle: generally, the larger the slope angle, the smaller the interaction factor.
(4) The influence of sloping ground on the dynamic interaction of pile and soil is associated with the vibration frequency and pile spacing. For a 2*d* pile spacing, topography has smaller influences on the real part of interaction factor with an increasing frequency. In contrast, for pile spacing of 5*d* and 10*d*, that monotonicity relies on the value of intersection frequency.

Declaration of Competing Interest

The authors declare that they have no known competing financial interests or personal relationships that could have appeared to influence the work reported in this paper.

Acknowledgements

This work was supported by the National Science Foundation of China (51878103, 51708064) and China Scholarship Council (File No: 201806050121) for financial support to visit Purdue University, the United States. Our deepest gratitude goes to the two anonymous referees for their valuable suggestions and thoughtful comments. We also acknowledge Dr. CS Goit of Saitama University, Japan for his efforts in improving the quality of this manuscript.

Appendix A. Brief derivation of the impedance of single piles partially embedded in slope ground

In Section 4.2, it's demonstrated that the slope topography exerts a neglectable influence on the vibration characteristics of single piles (also reported in Qu et al., 2020). Hence, the dynamic impedance of a single pile in the slope ground can be approximately replaced by the one in horizontal ground. The calculated model is shown in Fig. 24. The length of the whole pile shaft denotes L and is constituted by the unembedded segment L_1 and embedded segment L_2.

The vertical vibrating equilibrium of an element of the unembedded pile segment is written as:

$$E_pA_p\frac{\partial^2 u_1(z,t)}{\partial z^2}-m_p\frac{\partial u_1(z,t)}{\partial t^2}=0 \tag{A1}$$

$$u_1(z,t)=u_1(z)e^{i\omega t} \tag{A2}$$

where u_1 is the vertical displacement of the unembedded segment at a distance of z from the pile top at time t; E_p denotes the Young's modulus of the pile; A_p is the area of the pile cross section; m_p is the mass of the pile shaft per unit length; ω is the angular frequency of dynamic excitation; $i=\sqrt{-1}$

Substituting Eq. A2 into Eq. A1, one can obtain:

$$\frac{\partial^2 u_1(z)}{\partial z^2}+\frac{m_p\omega^2}{E_pA_p}u_1(z)=0 \tag{A3}$$

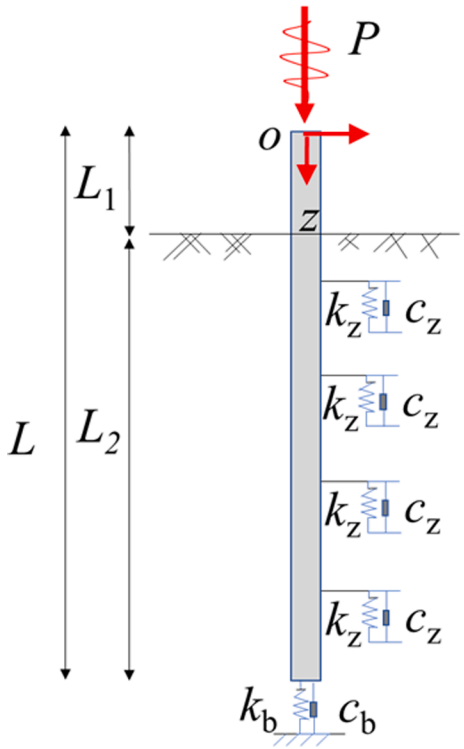

Fig. 24. Calculation model for the vertical vibration response of a partially embedded pile.

The general solution of Eq. A3 is:

$$u_1(z) = A_1 cos\left(\frac{\omega}{C_p} z\right) + B_1 sin\left(\frac{\omega}{C_p} z\right) \tag{A4}$$

The axial fore is given by:

$$N_1(z) = -E_p A_p \frac{\omega}{C_p}\left[-A_1 sin\left(\frac{\omega}{C_p} z\right) + B_1 cos\left(\frac{\omega}{C_p} z\right)\right] \tag{A5}$$

where A_1 and B_1 are undetermined coefficients.

Then, the dynamic pile impedance at the top of the unembedded segment can be expressed as:

$$Z(0) = \frac{N_1(0)}{u_1(0)} = -\frac{E_p A_p \frac{\omega}{C_p}}{\frac{A_1}{B_1}} \tag{A6}$$

Similarly, the dynamic pile impedance at bottom of the unembedded segment can be expressed as:

$$Z(L_1) = \frac{N_1(L_1)}{u_1(L_1)} = -\frac{E_p A_p \frac{\omega}{C_p}\left[-\frac{A_1}{B_1} tan\left(\frac{\omega}{C_p} L_1\right) + 1\right]}{\frac{A_1}{B_1} + tan\left(\frac{\omega}{C_p} L_1\right)} \tag{A7}$$

The vertical vibrating equilibrium of an element of the embedded pile segment can be written as:

$$E_p A_p \frac{d^2 u_2(z)}{dz^2} + m\omega^2 u_2(z) - \widetilde{k} u_2(z) = 0 \tag{A8}$$

where $u_2(z)$ is the vertical displacement of the embedded pile shaft at the elevation z; $\widetilde{k}$ is the complex soil stiffness calculated by $\widetilde{k} = k_z + i\omega c_z$ and the value of k_z and c_z can be referred in the study Gazetas et al. (1991).

Similar to that of the unembedded pile segment, the displacement and axial force of the embedded segment can be expressed as:

$$u_2(z) = A_2 cos(\lambda / C_p z) + B_2 sin(\lambda / C_p z) \tag{A9}$$

$$N_2(z) = -\frac{\lambda}{C_p} E_p A_p\left[-A_2 sin\left(\frac{\lambda}{C_p} z\right) + B_2 \frac{\lambda}{C_p} cos\left(\frac{\lambda}{C_p} z\right)\right] \tag{A10}$$

where $\lambda = \sqrt{\omega^2 - \widetilde{k}/\rho_p A_p}$

Thus, the dynamic impedance at the top of embedded pile segment can be expressed as:

$$Z(L_1) = \frac{N_2(L_1)}{u_2(L_1)} = -\frac{E_p A_p \frac{\lambda}{C_p}\left[-\frac{A_2}{B_2} tan\left(\frac{\lambda}{C_p} L_1\right) + 1\right]}{\frac{A_2}{B_2} + tan\left(\frac{\lambda}{C_p} L_1\right)} \tag{A11}$$

Considering the boundary condition at pile tip, one can obtain the following:

$$\frac{A_2}{B_2} = \frac{E_p \frac{\lambda}{C_p} + (k_b + i\omega c_b) tan\left(\frac{\lambda}{C_p} L\right)}{E_p \frac{\lambda}{C_p} tan\left(\frac{\lambda}{C_p} L\right) - k_b - i\omega c_b} \tag{A12}$$

Specially, when the soil under pile tip is uncompressible, Eq. (A12) can be simplified as:

$$\frac{A_2}{B_2} = -tan\left(\frac{\lambda}{C_p} L\right) \tag{A13}$$

Considering the consistency nature of the pile impedance at the ground horizontal ($z = L_1$), one has:

$$\frac{E_p A_p \frac{\omega}{C_p}\left[-\frac{A_1}{B_1} tan\left(\frac{\omega}{C_p} L_1\right) + 1\right]}{\frac{A_1}{B_1} + tan\left(\frac{\omega}{C_p} L_1\right)} = \frac{E_p A_p \frac{\lambda}{C_p}\left[-\frac{A_2}{B_2} tan\left(\frac{\lambda}{C_p} L_1\right) + 1\right]}{\frac{A_2}{B_2} + tan\left(\frac{\lambda}{C_p} L_1\right)} \tag{A14}$$

Substituting Eq. A13 into Eq. A14, the unknown coefficients can be given by:

$$\frac{A_1}{B_1} = \frac{\omega tan\left(\frac{\lambda}{C_p} L_1\right) - \lambda tan\left(\frac{\omega}{C_p} L_1\right) + \frac{A_2}{B_2}\left[\lambda tan\left(\frac{\lambda}{C_p} L_1\right) tan\left(\frac{\omega}{C_p} L_1\right) + \omega\right]}{\frac{A_2}{B_2}\left[\omega tan\left(\frac{\omega}{C_p} L_1\right) - \lambda tan\left(\frac{\lambda}{C_p} L_1\right)\right] + \lambda + \omega tan\left(\frac{\omega}{C_p} L_1\right) tan\left(\frac{\lambda}{C_p} L_1\right)} \tag{A15}$$

Combining with Eq. A6, the dynamic impedance at the top of the whole pile shaft can be formulated as:

$$Z(0)=\frac{E_pA_p\frac{\omega}{C_p}}{\frac{\omega tan\left(\frac{\lambda}{C_p}L_1\right)-\lambda tan\left(\frac{\omega}{C_p}L_1\right)+\frac{A_2}{B_2}\left[\lambda tan\left(\frac{\lambda}{C_p}L_1\right)tan\left(\frac{\omega}{C_p}L_1\right)+\omega\right]}{\frac{A_2}{B_2}\left[\omega tan\left(\frac{\omega}{C_p}L_1\right)-\lambda tan\left(\frac{\lambda}{C_p}L_1\right)\right]+\lambda+\omega tan\left(\frac{\omega}{C_p}L_1\right)tan\left(\frac{\lambda}{C_p}L_1\right)}} \tag{A16}$$

Specially, when the soil under pile tip is uncompressible, Eq. A16 can be simplified as:

$$Z(0)=\frac{E_pA_p}{L}\frac{\frac{L\omega}{C_p}\left[\frac{\lambda\psi}{\omega}+tan\left(\frac{\omega}{C_p}L_1\right)\right]}{1-\frac{\lambda\psi}{\omega}tan\left(\frac{\omega}{C_p}L_1\right)} \tag{A17}$$

Substituting Eq. A12 to Eq. A11, the dynamic impedance at the ground horizontal of the pile shaft can be written as:

$$Z(L_1)=\frac{N_2(L_1)}{u_2(L_1)}=\frac{E_pA_p\frac{\lambda}{C_p}\left[-\frac{E_p\frac{\lambda}{C_p}+(k_b+i\omega\ c_b)tan\left(\frac{\lambda}{C_p}L\right)}{E_p\frac{\lambda}{C_p}tan\left(\frac{\lambda}{C_p}L\right)-k_b+i\omega\ c_b}tan\left(\frac{\lambda}{C_p}L_1\right)+1\right]}{\frac{E_p\frac{\lambda}{C_p}+(k_b+i\omega\ c_b)tan\left(\frac{\lambda}{C_p}L\right)}{E_p\frac{\lambda}{C_p}tan\left(\frac{\lambda}{C_p}L\right)-k_b+i\omega\ c_b}+tan\left(\frac{\lambda}{C_p}L_1\right)} \tag{A18}$$

By combining Eq. A6 with Eq. A7, one can formulate the relationship between the displacements of the positions at the top and ground horizontal of the pile shaft:

$$u_1(L_1)=u_1(0)\left[cos\left(\frac{\omega}{C_p}L_1\right)+\frac{sin\left(\frac{\omega}{C_p}L_1\right)}{A_1/B_1}\right] \tag{A19}$$

References

Choudhury, D., Subba Rao, K.S., 2006. Seismic bearing capacity of shallow strip footings embedded in slope. Int. J. Geomech. 6 (3), 176–184.

Cui, C.Y., Meng, K., Wu, Y.J., Chapman, D., Liang, Z.M., 2018. Dynamic response of pipe pile embedded in layered visco- elastic media with radial inhomogeneity under vertical excitation. Geomech. Eng. 16 (6), 609–618.

Dobry, R., Gazetas, G., 1988. Simple method for dynamic stiffness and damping of floating pile groups. Géotechnique 38 (4), 557–574.

Di Benedetto, H., Doanh, T., Geoffroy, H., Sauzeat, C., 2003. Deformation Characteristics of Geomaterials. CRC Press.

Ding, X.M., Qu, L.M., Yang, J.C., Zheng, C.J., 2018. Vertical dynamic response of a pile embedded in viscoelastic soil considering the effects of lateral rigid boundary. In: Proceedings of IACGE. Chongqing. pp. 235–244.

Ding, X.M., Luan, L.B., Zheng, C.J., Mei, G.X., Zhou, H., 2019. An analytical solution for wave propagation in a pipe pile with multiple defects. Acta Mech. Solida Sin. https://doi.org/10.1007/s10338-019- 00123-5.

Gutowski, T.G., Dym, C.L., 1976. Propagation of ground vibration: a review. J. Sound Vib. 49 (2), 179–193.

Gazetas, G., Makris, N., 1991. Dynamic pile-soil-pile interaction. Part I: analysis of axial vibration. Earthquake Eng. Struct. Dyn. 20 (2), 115–132.

Gazetas, G., Fan, K., Kaynia, A., 1993. Dynamic response of pile groups with different configurations. Soil Dyn. Earthquake Eng. 12 (4), 239–257.

Han, F., Salgado, R., Prezzi, M., Lim, J., 2017. Shaft and base resistance of non-displacement piles in sand. Comput. Geotech. 83, 184–197.

Peng, Y., Liu, H.L., Li, C., Ding, X.M., Deng, X., Wang, C.Y., 2021. The detailed particle breakage around the pile in coral sand. Acta Geotech. https://doi.org/10.1007/s11440-020-01089-2.

Kaynia, A.M., Kausel, E., 1982. Dynamic Stiffness and Seismic Response of Pile Groups. Research Report. Department of Civil Engineering, MIT, Cambridge, Mass.

Kramer, S.L., 1996. Geotechnical Earthquake Engineering. Prentice Hall, Upper Saddle River, New Jersey.

Kouroussis, G., Verlinden, O., Conti, C., 2009. Ground propagation of vibrations from railway vehicles using a finite/infinite-element model of the soil. Proc. IME, Part F: J. Rail Rapid Transit 223 (4), 405–413.

Kouroussis, G., Anastasopoulos, I., Gazetas, G., Verlinden, O., 2013. Three-dimensional finite element modelling of dynamic pile-soil-pile interaction in time domain. In: Proceedings of 4th ECCOMAS Thematic Conference. Kos Island, Greece.

Kanellopoulos, K., Gazetas, G., 2019. Vertical static and dynamic pile-to-pile interaction in non-linear soil. Géotechnique 1–16.

Luco, J.E., Mita, A., 1987. Response of circular foundation to spatially random ground motion. J. Eng. Mech. 113 (1), 1–15.

Lin, Y.L., Yang, G.L., 2013. Dynamic behavior of railway embankment slope subjected to seismic excitation. Nat. Hazards 69 (1), 219–235.

Lei, G., Usai, S., Wu, W., 2019. Centrifuge study of soil arching in slope reinforced by piles. In: Wu, W. (Ed.), Recent Advances in Geotechnical Research. Springer Series in Geomechanics and Geoengineering. Springer, Cham. https://doi.org/10.1007/978-3-319-89671-7_9.

Li, Z.Y., Gao, Y.F., 2019. Effects of inner soil on the vertical dynamic response of a pipe pile embedded in inhomogeneous soil. J. Sound Vib. 439, 129–143.

Luan, L.B., Zheng, C.J., Kouretzis, G., Cao, G., Zhou, H., 2019. Development of a three-dimensional soil model for the dynamic analysis of end-bearing pile groups subjected to vertical loads. Int. J. Numer. Anal. Meth. Geomech. 43 (9), 1784–1793.

Luan, L.B., Ding, X.M., Zheng, C.J., Kouretzis, G., Wu, Q., 2020. Dynamic response of pile groups subjected to horizontal loads. Can. Geotech. J. 57 (4), 469–481.

Luan, L.B., Zheng, C.J., Kouretzis, G., Ding, X.M., 2020,. Dynamic analysis of pile groups subjected to horizontal loads considering coupled pile-to-pile interaction. Comput. Geotech. 117. https://doi.org/10.1016/j.compgeo.2019.103276.

Makris, N., Gazetas, G., 1993. Displacement phase differences in a harmonically oscillating pile. Géotechnique 43 (1), 135–150.

Mylonakis, G., Gazetas, G., 1998. Vertical vibration and additional distress of grouped piles in layerd soil. Soils Found. 38 (1), 1–14.

Nontapat, N., Yohsuke, K., Deepak, R., et al., 2018. Full-scale tests on effects of slope on lateral capacity of piles installed in cohesive soils. J. Geotech. Geoenviron. Eng. https://doi.org/10.1061/(ASCE)GT.1943-5606.0001805.

Poulos, H.G., 1968. Analysis of the settlement of pile groups. Géotechnique 18 (4), 449–471.

Peplow, A.T., Jones, C.J., Petyt, M., 1999. Surface vibration propagation over a layered elastic half-space with an inclusion. Appl. Acoust. 56 (4), 283–296.

Qu, L.M., Ding, X.M., Zheng, C.J., Liu, H.L., 2017. An analytical solution for wave propagation in a square pile due to transient point load. Comput. Geotech. 83, 77–82.

Qu, L.M., Ding, X.M., Wu, C.R., Long, Y.H., Yang, J.C., 2020. Effects of topography on dynamic responses of single piles under vertical cyclic loading. J. Mountain Sci. 17 (1), 230–243.

Randolph, M.F., Wroth, C.P., 1978. Analysis of deformation of vertically loaded piles. J. Geotechn. Eng. Div. 104 (12), 1465–1488.

Srbulov, M., 2010. Ground Vibration Engineering: Simplified Analyses With Case Studies and Examples. Springer Science & Business Media.

Tripe, R., Kontoe, S., Wong, T.K.C., 2013. Slope topography effects on ground motion in the presence of deep soil layers. Soil Dyn. Earthquake Eng. 50, 72–84.

Ullah, M.S., Yamamoto, H., Goit, C.S., Saitoh, M., 2018. On the verification of superposition method of kinematic interaction and inertial interaction in dynamic response analysis of soil-pile-structure systems. Soil Dyn. Earthquake Eng. 113, 522–533.

Van Baars, S., 2014. The inclination and shape factors for the bearing capacity of footings. Soils Found. 54 (5), 985–992.
Wolf, J.P., Von Arx, G., 1978. Impendance function of a group of vertical piles. Pasadena, California: Earthquake Engineering and Soil Dynamics, the ASCE Geotechnical Engineering Division Specialty Conference.
Wolf, J.P., 1998. Simple physical models for foundation dynamics. Develop. Geotechn. Eng. Elsevier 83, 1–70.
Wu, W.B., Liu, H., Yang, X., Jiang, G.S., El Naggar, M.H., Mei, G., Liang, R., 2020. New method to calculate the apparent phase velocity of open-ended pipe pile. Can. Geotech. J. 57 (1), 127–138.
Zhang, S., Cui, C.Y., Yang, G., 2019. Vertical dynamic impedance of pile groups partially embedded in multilayered, transversely isotropic, saturated soils. Soil Dyn. Earthquake Eng. 117, 106–115.
Zhao, M.H., Yang, C.W., Yang, M.H., et al., 2014. Mechanical analysis of bridge pile foundation in high and steep slopes based on finite bar element method. China J. Highway Transp. 27 (6), 51–58+108 [in Chinese].
Zhou, P., Zhou, H., Liu, H.L., Li, X.Y., Ding, X.M., Wang, Z.L., 2020. Analysis of lateral response of existing single pile caused by penetration of adjacent pile in undrained clay. Comput. Geotech. https://doi.org/10.1016/j.compgeo.2020.103736.